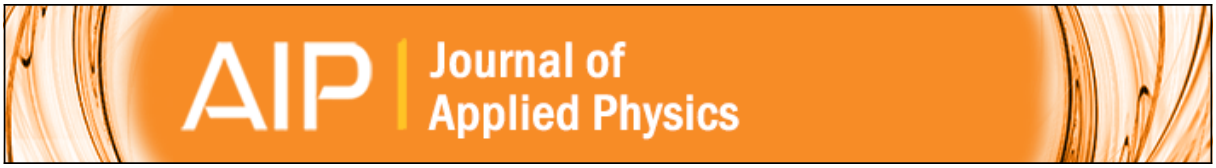

Sensitivity enhancement in thermoreflectance microscopy of semiconductor devices using suitable probe wavelengths

L. R. de Freitas, E. C. da Silva, A. M. Mansanares, G. Tessier, and D. Fournier

Citation: Journal of Applied Physics **98**, 063508 (2005); doi: 10.1063/1.2043231

View online: http://dx.doi.org/10.1063/1.2043231

View Table of Contents: http://scitation.aip.org/content/aip/journal/jap/98/6?ver=pdfcov

Published by the AIP Publishing

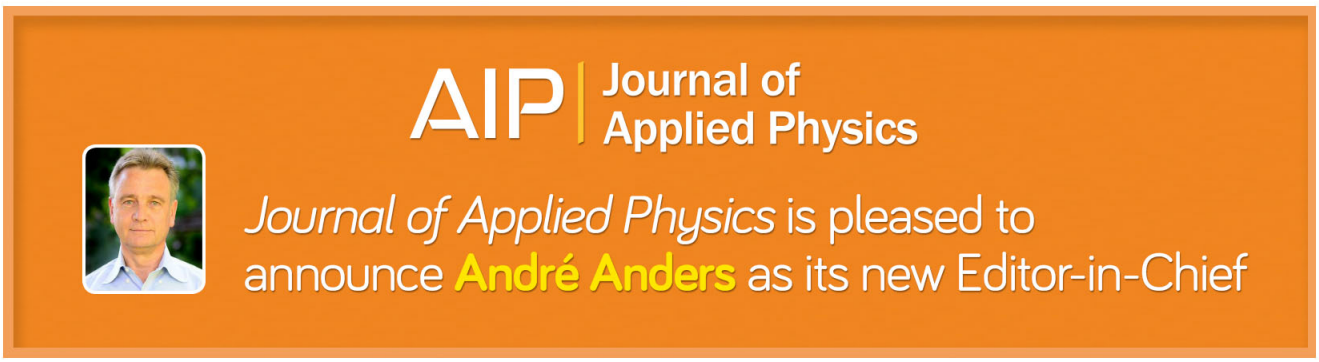

Sensitivity enhancement in thermoreflectance microscopy of semiconductor devices using suitable probe wavelengths

L. R. de Freitas, E. C. da Silva, and A. M. Mansanares[a)]
Instituto de Fisica Gleb Wataghin, Universidade Estadual de Campinas, Unicamp, Cx.P. 6165, 13083-970, Campinas, São Paulo, Brazil

G. Tessier and D. Fournier
Laboratoire d'Instrumentation, Université Pierre et Marie Curie (UPMC), Unité Propre de Recherche (UPR) A0005 du Centre National de la Recherche Scientifique (CNRS), Ecole Supérieure de Physique et de Chimie Industrielles de la Ville de Paris (ESPCI), 10 rue Vauquelin, 75005 Paris, France

(Received 14 February 2005; accepted 3 August 2005; published online 20 September 2005)

In this paper we present an experimental and theoretical study of the thermoreflectance response as a function of the probe wavelength for layered microelectronics structures. The investigated sample consists of a polycrystalline silicon conducting track grown on a SiO_2-coated Si substrate. Thermoreflectance measurements were carried out in the wavelength range from 450 to 750 nm with the track biased in modulated regime. An oscillating pattern is observed in the spectral region where the upper layer is transparent. Such oscillations are due to the interference resulting from the multiple reflections at the interfaces. Using a thermo-optical model, we show that the optical constants (n and k) of the materials, which are wavelength dependent, as well as their temperature derivatives (dn/dT and dk/dT), strongly influence the thermoreflectance signal. The optical thicknesses of the layers, mainly determined by the real part of the refractive indices, define the period of oscillation. On the other hand, the imaginary part of the refractive indices establishes the cutoff wavelength of the oscillations. Below this cutoff wavelength, the probe light does not penetrate the material and the upper-surface reflectance dominates the signal. © *2005 American Institute of Physics*. [DOI: 10.1063/1.2043231]

I. INTRODUCTION

Thermoreflectance microscopy has been used during the last decade as a suitable technique for the investigation of micro- and opto-electronic devices in operating cycle.[1–16] It allows the determination of both heat source distribution and heat propagation properties within specific regions of micrometer devices. The technique is also useful for detecting and imaging defects. Besides the temperature field, it is also sensitive to local electric field,[1] as well as to free-carrier density, which are in their turn disturbed by defects. The noncontact and nondestructive character of the technique is one of its main advantages. It enables aging tests, which are a necessary step in the development of electronic devices, as well as progressive and repetitive treatments such as the application of voltage pulses intended to simulate electrostatic discharge damaging.[2]

The technique has been applied in the investigation of operating telecommunication diode lasers,[3–6] transistors,[7–9] interconnects,[10,11] and solar cells.[12] Sensitivity and spatial resolution ensures the capability of the technique to sense temperature profile variation due to both structural differences and local surface/subsurface defects at micrometer and, in some cases, even at submicrometer scales. In some applications, however, the sensitivity drops down due to the material's optothermal properties. In this case, the choice of appropriate experimental conditions, such as specific probe wavelength, is crucial to preserve the signal-to-noise ratio and guarantee reliable measurements.

In this paper we present a systematic study of the dependence of the thermoreflectance response with the probe wavelength for a layered structure consisting of a conducting track made on a Si substrate. The conducting track and substrate are isolated by a silicon oxide layer. Thermoreflectance measurements were carried out in the wavelength range from 450 to 750 nm with the polycrystalline silicon track biased in the modulated regime (ac voltage applied to the track pads). Using a thermo-optical model, we show that the optical constants (n and k) of the materials, which are wavelength dependent, as well as their temperature derivatives (dn/dT and dk/dT), strongly influence the thermoreflectance signal (see Ref. 17 for thermal and wavelength modulation spectroscopies). An oscillating pattern is observed in the spectral region where the upper layer is transparent. Such oscillations are due to the interference resulting from the multiple reflections at the interfaces. The optical thicknesses of the layers determine the period of oscillation.

A remarkable aspect of these oscillations is the fact that, when scanning the sample surface, one can pass from a situation where the reflectance increases to another where the reflectance decreases with temperature, depending on the thicknesses of the layers and on the materials of each region. The signal phase is then shifted by 180° from one case to another, and therefore a superb contrast between a selected part of the structure and its neighborhood can be achieved.

[a)]Electronic mail: manoel@ifi.unicamp.br

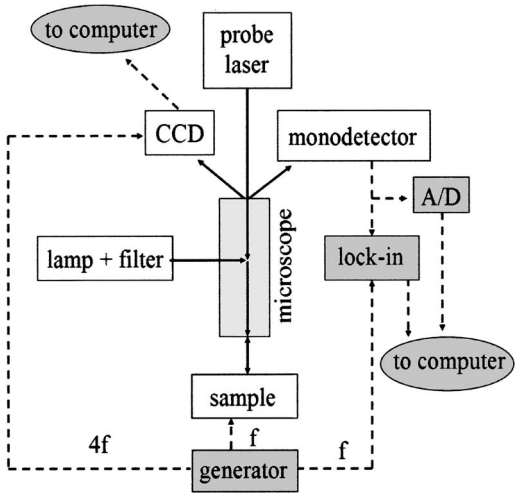

FIG. 1. Block diagram of the combined arrangement: focused laser and CCD camera setups.

II. EXPERIMENT

We used two experimental setups, namely, the visible charge-coupled device (CCD) camera setup,[14–16] which uses a lamp to produce the probe light and stores the whole thermal image in a snapshot, and the focused laser setup,[8] which uses several laser lines as probe and stores the thermal image by scanning the sample surface. The two experimental setups are depicted in the block diagram of Fig. 1.

In the CCD technique, the sample is continuously illuminated by a white light that passes through an interference filter (linear variable filter), which allows specific wavelength tuning in the visible region (the range used in this work, with this setup, was 500–800 nm). A function generator supplies a modulated voltage to the sample at a fixed frequency f and a second generator provides a signal to the camera, synchronized with the former, at four times the fixed frequency $(4f)$. The CCD camera acquires a series of four different images, each one integrated over one-fourth of the period of the heating modulation. In this way, through simple math one obtains the amplitude and phase of the thermoreflectance signal.[18] To improve the signal-to-noise ratio, accumulation of these images is done. The CCD image is composed of 1024×1024 pixels. Each pixel corresponds to 88×88 nm when using a $100\times$ objective, so the whole image in this case is 90×90 μm. The modulation frequency is limited in this arrangement to 7.5 Hz (which is the frequency used in the measurements presented below), since the maximum CCD frame rate is 30 Hz.

In the focused laser setup, a probe-laser beam is focused on the sample surface. The spot diameter is about 1.0 μm ($50\times$ objective with numerical aperture (NA)=0.75). The beam is reflected back by the surface of the sample and deviated to a Si photodiode (monodetector) by using a $\lambda/4$ plate combined with a polarizing beam splitter cube. The output signal from the Si detector is lock-in analyzed (reference in-phase with the generator driving voltage). The sample is mounted on an x-y translation stage of step size of 0.1 μm in order to scan the probe beam on its surface. The probe-laser wavelengths used in this work are those of Ar^+ laser lines (457.9, 476.5, 488.0, 496.5, 501.7, and 514.5 nm) and 670 nm coming from a diode laser. The modulation frequency in this arrangement can vary from 1.0 kHz to a few megahertz. The results presented below were obtained at 100 kHz.

The modulated voltage applied to the sample has the form $V(t)=(V_0/2)[1+\sin(2\pi ft)]$, with $V_0=5.0$ V in all the measurements. The reflected probe beam, in both arrangements, is intensity modulated at frequency f, since the sample″s reflectance (R) is a function of temperature T, which is modulated as well due to the current flow and voltage modulations. For the particular waveform of the applied voltage above, there is joule dissipation at the frequency f and at $2f$ as well. Only the f component was captured by the lock-in. The ac output signal from the CCD (or from the Si detector) is normalized by its dc component, giving the experimental values of $\Delta R/R$:

$$\frac{\Delta R}{R}=\frac{S_{\mathrm{ac}}}{S_{\mathrm{dc}}}=\frac{1}{R}\frac{\partial R}{\partial T}\Delta T. \tag{1}$$

Photogenerated carriers can also contribute to the reflectance change. In our case, the probe beam does penetrate the polycrystalline silicon layer, eventually reaching the Si substrate, being then completely absorbed. Photocarriers in the substrate do not oscillate at frequency f, since the probe beam is not modulated. On the other hand, photocarriers created within the polycrystalline silicon layer are driven by the applied voltage and may contribute to the signal.[7] Such a contribution is, however, negligible in our case, since the signal amplitude follows a quadratic dependence on V_0 (not shown), which ensures that the main mechanism of signal generation is the joule effect.

In the case of the focused laser setup, the probe beam intensity at the detector is of the order of 10^{-4}–10^{-5} W, which gives a signal-to-noise ratio of roughly $10^6/\sqrt{\mathrm{Hz}}$, high enough to comfortably detect the features of the thermoreflectance signal in microelectronics structures. Typical responses of biased devices are in the range of 10^{-3}–10^{-5} in $\Delta R/R$.[13] However, in the case of the CCD camera, the signal-to-noise ratio is at least two orders of magnitude smaller for a single acquisition. In this case, the accumulation of images is necessary. Usually a few hundred images are enough to reach a comfortable signal-to-noise ratio.

The main advantages of the CCD technique are the faster data acquisition (13 s for 400 images at 30 Hz) and the easy tuning ability obtained by using the linear variable interference filter. On the other hand, the focused laser technique has the capability of performing measurements in high modulation frequencies using simple homodyne detection and presents higher sensitivity.

Besides thermoreflectance measurements $(\Delta R/R)$, we also performed measurements of the reflectance R as a function of the wavelength in the range of 500–800 nm using a spectrophotometer coupled to the eyepiece of the microscope. In this case the sample was illuminated with white light and the reflected beam was dispersed by the spectrophotometer. The measurement of the sample reflectance served as support for the modeling of the thermoreflectance problem, as presented below.

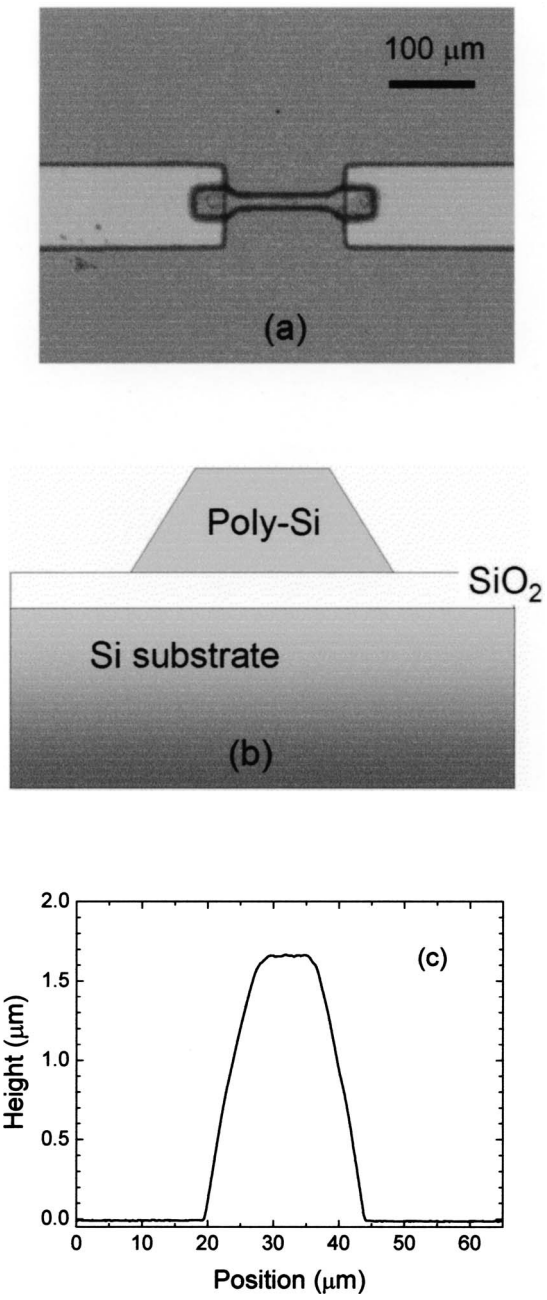

FIG. 2. (a) Photomicrograph of the conducting track, (b) schematics of the cross section of the sample, and (c) profile of the track showing its height and width.

Several samples with distinct conducting tracks (geometry, thickness, material) were investigated. The results described below were obtained on a polycrystalline silicon track grown on a crystalline *n*-Si substrate. The track is 1.6 μm thick, 25 μm wide, and 200 μm long, and it is isolated from the substrate by a 0.5-μm SiO_2 layer. The polycrystalline silicon layer is made of phosphorous-doped (10^{20} atoms/cm^3) silicon. Figure 2 shows a photomicrograph of the track [Fig. 2(a), lateral contacts are made of Al], the schematics of the cross section of the sample [Fig. 2(b)], and the measurement of the height and width of the track performed with a profilometer [Fig. 2(c)].

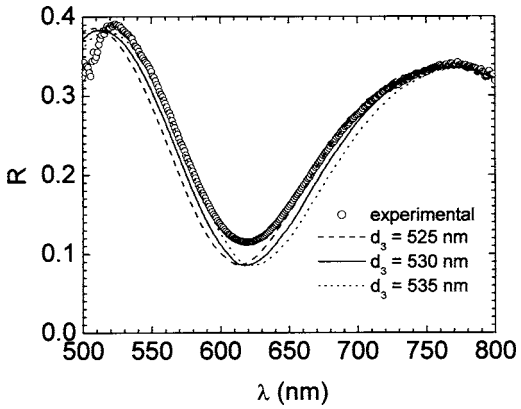

FIG. 3. Reflectance as a function of the wavelength measured on the substrate coated with the SiO_2 layer (open circles) and calculated reflectance for three values of the SiO_2 thickness (d_3).

III. RESULTS

Figure 3 shows the reflectance R as a function of the wavelength (open circles), measured on the substrate coated with the SiO_2 layer, i.e., far from the conducting track. The interference pattern observed is caused by the combination of the reflected rays at the air/SiO_2 and SiO_2/Si substrate interfaces. The lines (dashed, solid, and dotted) represent the calculated reflectance for distinct values of the SiO_2 thickness. Detailed discussion is found in Sec. IV.

Figure 4(a) presents the same measurement obtained on the polycrystalline silicon track (open circles). It can be seen that, besides the low spatial frequency pattern observed in Fig. 3 (envelope), there is also a higher spatial frequency pattern that is related to the additional polycrystalline silicon layer, as will be discussed in Sec. IV. It is also observed that the high-frequency oscillation almost disappears for smaller wavelengths. The reason is that the polycrystalline silicon becomes absorbing at short wavelengths, thus extinguishing the multiple reflections at the inner interfaces (polycrystalline silicon/SiO_2 and SiO_2/Si substrate).

A whole optical image, obtained through the reflectance of the sample under illumination with $\lambda = 650$ nm, using the CCD camera setup, is presented in Fig. 5(a). In this image one can see a zoom of Fig. 2(a), with the difference that here the illumination is done with monochromatic light. Therefore, the bright/dark levels of Fig. 5(a) represent the reflectance of the distinct regions of the sample at 650 nm. One can observe the high reflectance of the Al contact at the left side, the middle level reflectance of the conducting track, and the lower reflectance level of the SiO_2-covered substrate. A thermoreflectance image ($\Delta R/R$), obtained using 650 nm as probe wavelength, is shown in Fig. 5(b). In this image one can clearly see the heated polycrystalline silicon track (bright). It must be noticed that the Al contact presents a very low level of thermoreflectance signal amplitude (dark), which results from the lower temperature changes, due to the higher thermal and electrical conductivities of Al, besides the larger width of the contact. Nevertheless, the temperature coefficient of the reflectance also influences the contrast between the Al contact and the polycrystalline silicon track. The observed differences in brightness between the upper

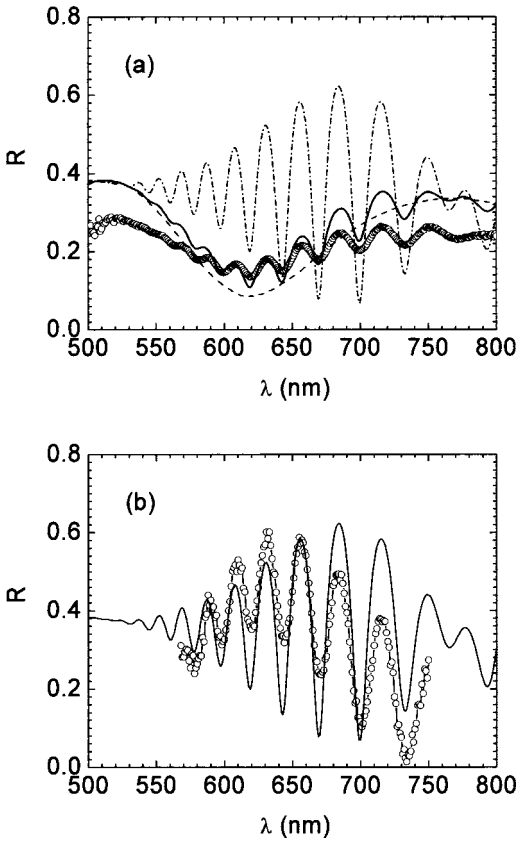

FIG. 4. (a) Reflectance as a function of the wavelength measured on the polycrystalline silicon track (open circles), calculated reflectance of the whole structure including the conducting track (1600-nm thick, dashed-dotted curve), and calculated average reflectance (20% track-80% coated substrate, solid line). The dashed curve represents the calculated reflectance for the coated substrate (same as in Fig. 3 for $d_3=530$ nm), (b) calculated reflectance of the whole structure (solid line), and corrected experimental points resulting in the reflectance coming exclusively from the track (20% track-80% coated substrate, open circles).

and the lower parts of the Al pad must be caused by the nonuniformity of the pad thickness (slanted surface). Care was taken of the sample alignment. A Mirau lens was used to ensure that the substrate surface was actually perpendicular to the incident probe light beam.

Figure 6 presents the thermoreflectance signal, $\Delta R/R$, on the center of the polycrystalline silicon track (averaged over a 1.0-μm-diameter spot), for several wavelengths, namely,

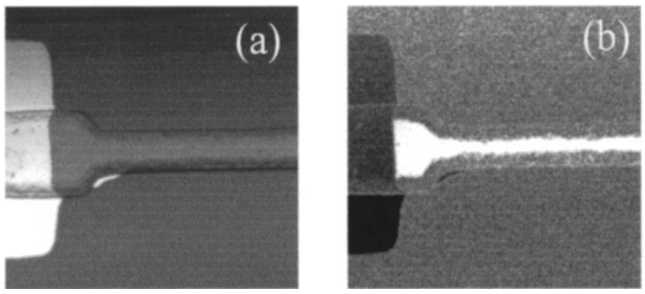

FIG. 5. (a) Optical image of the conducting track obtained through the reflectance of the sample under illumination with 650 nm, obtained using the CCD camera setup; (b) CCD camera thermoreflectance image ($\Delta R/R$) obtained using 650 nm as probe wavelength. Dark means zero and bright means maximum signal amplitude ($\Delta R/R=2.4\times10^{-2}$). Scanned area is 70 $\times 70$ μm^2.

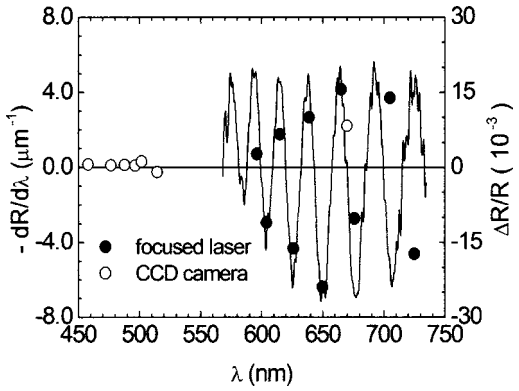

FIG. 6. Experimental values of $\Delta R/R$ for several probe wavelengths (circles), and minus the derivative of the experimental reflectance of the conducting track (raw data) with respect to the wavelength.

all the laser lines listed above (focused laser setup, open circles) and at 596, 604, 615, 626, 639, 650, 665, 676, 705, and 725 nm (CCD camera setup, closed circles). Negative and positive values of $\Delta R/R$ are used to represent in-phase and 180° out-of-phase thermoreflectance signal. The choice of the wavelengths in the CCD camera setup was made using the derivative of the reflectance of the conducting track with respect to the wavelength. Around the maximum of the derivative (absolute value) it is expected that the thermoreflectance is also a maximum, since one of the effects of increasing temperature is to change the optical path inside each layer, thus shifting the interference pattern. Furthermore, the optical spectra of the materials usually present a redshift with increasing temperature, besides the broadening of their bands.[17] The numerical derivative of the measured reflectance of the conducting track [open circles in Fig. 4(a)] is plotted in Fig. 6 (solid line) to evidence its maximum-value wavelengths, at which the thermoreflectance measurements were performed.

From $\Delta R/R$ measurements of Fig. 6 one can see that the thermoreflectance response is significantly enhanced above 600 nm and a net oscillating pattern is observed at higher wavelengths. This oscillating pattern is closely connected to the interference oscillations observed in the reflectance spectrum as we will see in the theoretical model below.

IV. THEORETICAL MODEL AND DISCUSSION

The theoretical model we developed to analyze the thermoreflectance response is based on the thermal modulation of the reflectance that results from the multiple reflections of the probe beam in the layered structure. This modulation comes from the temperature dependence of the refractive indices of the materials, as well as from the thickness variation due to thermal expansion. In all the calculations, the temperature variation was considered uniform throughout all the interfaces, i.e., temperature gradient was neglected. Let us remind that the heat source is located within the polycrystalline silicon track. Beneath the track, the oscillating temperature amplitude decreases roughly with the factor $e^{-d/\mu}$, where d is the distance from the track (heat source) and μ is the thermal diffusion length.[11] The values for μ using literature data[11] are $\mu_{Si}(100\ \text{kHz})=16\ \mu\text{m}$ and $\mu_{SiO_2}(100\ \text{kHz})$

TABLE I. Optical constants and their temperature derivatives at 500 and 800 nm, and the thermal-expansion coefficient for crystalline silicon, polycrystalline silicon, and silicon oxide.

Material	n	k	dn/dT (10^{-4} K^{-1})	dk/dT (10^{-4} K^{-1})	α_T (10^{-6} K^{-1})
Si at 500 nm	4.3[a,b]	0.023	2.9[a–c]	2.2	
Si at 800 nm	3.7	0.006	0.61	0.61	
Poly-Si at 500 nm	4.2[d]	0.13			2.6[e]
Poly-Si at 800 nm	3.7	0.006			
SiO_2 at 500 nm	1.462[f]		0.13[g]		0.55[h]
SiO_2 at 800 nm	1.453				

[a]Reference 19.
[b]Reference 20.
[c]Reference 21.
[d]Reference 22.
[e]Reference 26.
[f]Reference 23.
[g]Reference 25.
[h]Reference 27.

$=1.6$ μm, which are large enough when compared to the layer thicknesses, thus ensuring the pertinence of the uniform temperature assumption.

Therefore, a first attempt was to describe the reflectance behavior as a function of the wavelength for both the SiO_2-coated substrate and for the whole structure (two layers on the substrate). Indeed, the model consisted of four media: medium 1: air; medium 2: polycrystalline silicon layer; medium 3: SiO_2 layer; and medium 4: Si substrate. For simplicity the refractive index of air was fixed ($n_1=1$ for the whole wavelength range) and considered temperature independent. The refractive indices (n and k) for silicon (polycrystalline track and crystalline substrate), and (n) for the silicon oxide layer, were taken from Refs. 19 and 20, 22, and 23, for each wavelength in the 500–800-nm range (interpolated values). Values of n ranged from 4.2 to 3.7 for polycrystalline silicon, while k values ranged from 0.13 to 0.006 when going from 500 to 800 nm. For crystalline silicon, n varies from 4.3 to 3.7 over the same wavelength range, while k goes from 0.023 to 0.006. The values of n for SiO_2 decrease from 1.462 to 1.453, following the Cauchy equation. [24] See Table I for a summary of the input data for calculations.

The reflectance of the four-media system was calculated considering the multiple reflections of a beam under normal incidence. The reflectance R is given by

$$R = \hat{r}^* \hat{r}, \tag{2}$$

where $\hat{r}$ is the reflection Fresnel coefficient given by the ratio between the reflected (E'_{1s}) and the incident (E_{1s}) electric-field amplitudes (we assumed normal incidence, so s and p polarizations are equivalent; actually, circularly polarized laser light and nonpolarized white light were used):

$$\hat{r} = \frac{E'_{1s}}{E_{1s}}. \tag{3}$$

Incident, reflected, and transmitted (E_{4s}) electric fields are related by the matrix equation below:[24]

$$\begin{pmatrix} E_{1s} \\ E'_{1s} \end{pmatrix} = C_1 C_2 C_3 \begin{pmatrix} E_{4s} \\ 0 \end{pmatrix}, \tag{4}$$

where

$$C_i = \frac{1}{\hat{t}_{i,i+1}} \begin{pmatrix} e^{-i\hat{\beta}_i/2} & \hat{r}_{i,i+1} e^{-i\hat{\beta}_i/2} \\ \hat{r}_{i,i+1} e^{i\hat{\beta}_i/2} & e^{i\hat{\beta}_i/2} \end{pmatrix} \tag{5}$$

and $\hat{r}_{i,i+1}$ and $\hat{t}_{i,i+1}$ are the reflection and transmission Fresnel coefficients at the interface between media i and $(i+1)$ for s polarization,[24] while $\hat{\beta}_i = 4\pi \hat{n}_i d_i / \lambda$ is the complex phase shift introduced by layer i, with $\hat{\beta}_1 = 1$. Here, $\hat{n}_i = (n_i + ik_i)$ is the complex refractive index of medium i, d_i is the thickness of layer i, and λ is the wavelength of the incident beam in air (vacuum).

As mentioned above, Fig. 3 presents the calculated reflectance for the Si substrate coated with a SiO_2 layer. The nominal thickness of the silicon oxide layer is 0.5 μm, and the calculation made for three values of the thickness d_3 (525, 530, and 535 nm) is shown in Fig. 3. One can see that the value of 530 nm best fits the experimental data. It must be noticed that both measured and calculated data are raw, no adjusting factors were employed. The agreement between experiment and calculation is quite satisfactory.

In the same way, the reflectance of the whole structure, including the polycrystalline silicon conducting track (1600 nm thick), was calculated and is plotted in Fig. 4(a) (dashed-dotted curve). The high spatial frequency previously observed in the experimental data obtained on the conducting track is clearly present in the calculated curve. The correct number of peaks and their positions are determined by the thickness of the polycrystalline silicon layer. Indeed, the best agreement with experiment is achieved for $d_2 = 1600$ nm. It is also remarked that the amplitude of the oscillations decreases at small wavelengths, and it is enveloped by the reflectance of the coated substrate, as expected. The disagreement with the measurement arises from the fact that the measured reflectance results from an average of the reflections that occur on the conducting track and on the surrounding substrate (coated with SiO_2). This comes out because the collecting optics of the spectrophotometer inspects a region that is larger than the track area. Therefore, in order to compare with the experiment, the calculated reflectance also must be averaged in the same way. An estimated proportion between track and substrate areas under inspection by the spectrophotometer is 20%–80%. Doing such averaging one obtains the solid line of Fig. 4(a), which qualitatively agrees quite well with experiment. The quantitative agreement is also reasonable considering other nonideal aspects such as track edge, nonuniformity of layer thickness, literature values used for the optical constants, non-normal incidence of the probe light beam, etc.

Once the reflectance modeling was accomplished, the next step is to add the effect of temperature modulation. This must be done exclusively on the conducting track, i.e., without considering the disturbance coming from the surroundings, as discussed above, since the thermoreflectance data were collected only on the center of the track. Let us remember that the CCD camera, as well as the focused laser optics, has submicrometric resolution, allowing picking the thermoreflectance signal in a small region at the center of track. Therefore, the reflectance curve that must be modulated by temperature in further calculations is the one represented in

Fig. 4(a) by the dashed-dotted line. This curve is plotted again in Fig. 4(b) with the experimental points properly corrected. This correction is in fact the reverse operation performed with the theoretical data of Fig. 4(a), i.e., the substrate contribution to the experimental data was taken off. So, experimental and theoretical plots of Fig. 4(b) represent the reflectance of the four-media structure.

From Eq. (1) one can see that the dependence of $\Delta R/R$ with the wavelength comes from the temperature coefficient of the reflectance, $(1/R)(\partial R/\partial T)$. In order to compute this coefficient, the reflectance was calculated at ambient temperature T as presented above, and then recalculated at the temperature $(T+\Delta T)$. The ratio $(\Delta R/\Delta T)$ equals the derivative $(\partial R/\partial T)$ in the limit of small values of ΔT:

$$\frac{\partial R}{\partial T} = \frac{\Delta R}{\Delta T} = \frac{R(T+\Delta T) - R(T)}{\Delta T}. \tag{6}$$

The reflectance $R(T+\Delta T)$ was calculated using values of $\hat{n}_i(T+\Delta T)$ and $d_i(T+\Delta T)$ given by

$$\hat{n}_i(T+\Delta T) = \hat{n}_i(T) + \frac{\partial \hat{n}_i}{\partial T}\Delta T, \tag{7}$$

$$d_i(T+\Delta T) = d_i(T)(1+\alpha_{Ti}\Delta T). \tag{8}$$

In the above equations $(\partial \hat{n}_i/\partial T) = (\partial n_i/\partial T + i\partial k_i/\partial T)$ is the complex temperature coefficient of the refractive index and α_{Ti} is the thermal expansion coefficient of material i. The values of $(\partial n/\partial T)$ and $(\partial k/\partial T)$ for crystalline silicon were taken from Refs. 13 and 19–21. The same values were used for polycrystalline silicon. They ranged from $(\partial n/\partial T) = 2.9 \times 10^{-4}\ \mathrm{K}^{-1}$ and $(\partial k/\partial T) = 2.2 \times 10^{-4}\ \mathrm{K}^{-1}$ at 500 nm to $(\partial n/\partial T) \cong (\partial k/\partial T) = 6.1 \times 10^{-5}\ \mathrm{K}^{-1}$ at 800 nm. For silicon oxide, $(\partial n/\partial T)$ is almost constant in the wavelength range and equal to $1.3 \times 10^{-5}\ \mathrm{K}^{-1}$.[25] The values of the thermal expansion coefficients of polycrystalline silicon and silicon oxide used were $2.6 \times 10^{-6}\ \mathrm{K}^{-1}$ (Ref. 26) and $5.5 \times 10^{-7}\ \mathrm{K}^{-1}$,[27] respectively (see Table I). Indeed, the calculation was expanded down to 450 nm to cover the measurements done using the laser lines.

Figure 7(a) shows the calculated curve of $\Delta R/\Delta T$. As in the case of the thermoreflectance measurements, it presents the oscillating pattern that is attenuated at small wavelengths. Figure 7(b) displays the coefficient $(1/R)(\Delta R/\Delta T)$ with the experimental data for the thermoreflectance $\Delta R/R$, properly normalized to best fit the calculated curve. Notice that $\Delta R/R$ and $(1/R)(\Delta R/\Delta T)$ are connected by the temperature variation ΔT [see Eq. (1)], so ΔT value was adjusted to find the best agreement between theory and experiment.

As one can see, theory and experiment present a very good accord, despite the simplifications in the model (normal incidence, uniform temperature) and inherent errors in the employed parameters (refractive indices and their temperature derivatives, thickness, thermal-expansion coefficients). The calculated curve shows, however, that the maxima of the thermoreflectance signal do not coincide with the maxima of $(dR/d\lambda)$, as guessed during measurements (see Fig. 6). In fact, the calculated maxima are slightly shifted to longer wavelengths, so the measured points do not fall precisely on

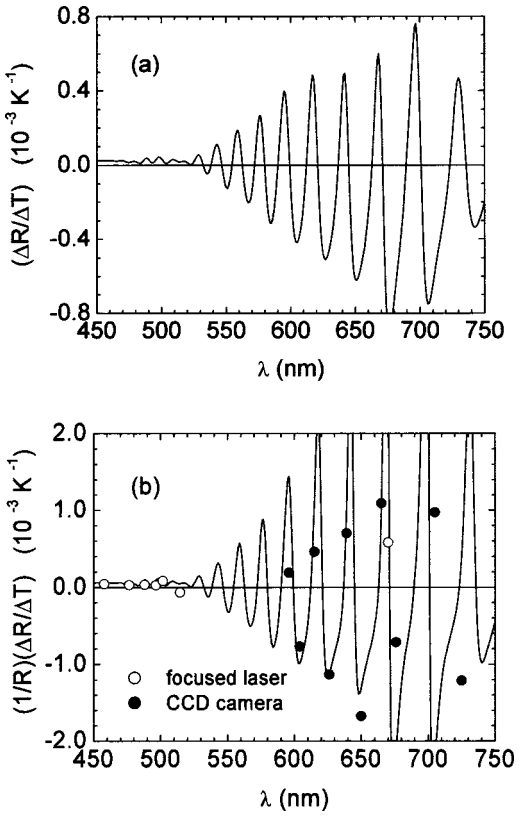

FIG. 7. (a) Calculated values of $\Delta R/\Delta T$ as a function of the wavelength; (b) calculated coefficient $(1/R)(\Delta R/\Delta T)$ (solid line) and experimental data for the thermoreflectance $\Delta R/R$ (circles), properly normalized to best fit the calculated curve.

the peaks of the calculated curve. In other words, the choice of the probe wavelengths could be done in such a way that would result in even more enhanced responses.

For the sake of comparison, the theoretical calculation of $(-1/R)(dR/d\lambda)$ is plotted in Fig. 8 with the curve for $(1/R)(\Delta R/\Delta T)$, where one can see the cited wavelength shift. The connection between $(\partial R/\partial T)$ and $(dR/d\lambda)$ arises from the fact that augmenting the temperature results in an increase of the optical path $(n_i d_i)$ within the polycrystalline silicon and silicon oxide layers. Since the interference peaks are determined by the ratio of $(n_i d_i/\lambda)$, it is easy to see that an augmentation of the optical path has an effect similar to that of a decrease in the wavelength λ. Consequently, there is

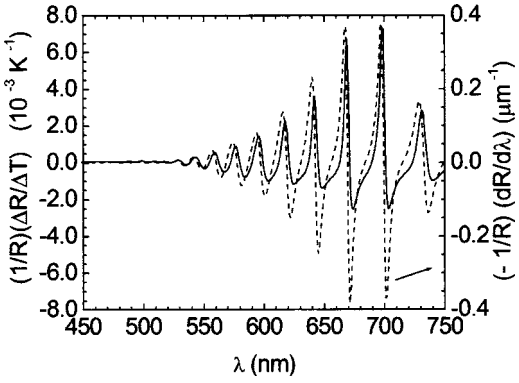

FIG. 8. Theoretical calculation of $(-1/R)(dR/d\lambda)$ (dashed line) and $(1/R) \times (\Delta R/\Delta T)$ (solid line), as functions of the wavelength.

an analogous behavior of $(\partial R/\partial T)$ and $(-dR/d\lambda)$, although slight differences come out from the distinct dependences of the phase shift, $\hat{\beta}$, on $n_i d_i$ and on λ, as well as from the fact that the refractive indices themselves influence the reflectance through the Fresnel coefficients $\hat{r}$ and $\hat{t}$.

Finally, one can say that the thermoreflectance signal in microelectronics structures and devices is strongly dependent on the probe wavelength, especially when the upper layers are transparent to the probe light. Optical interference, which is thermally modulated, plays a decisive role in the thermoreflectance response. The appropriate choice of the probe wavelength may strongly enhance the sensitivity of the technique. In the present case, the polycrystalline silicon layer defined the interference pattern, i.e., the spatial frequency was established by the track optical thickness, and the stronger optical absorption of this material at smaller wavelengths imposed the attenuation in the oscillating pattern and the loss of sensitivity in this wavelength range, as observed in the experiments.

V. CONCLUSIONS

In this paper we presented both experimental results and theoretical calculations of the dependence of the thermoreflectance response with the probe wavelength for a layered microelectronics structure. Experiments were carried out using two distinct arrangements, namely, the CCD camera and the focused laser setups, covering the spectral range from roughly 450 to 750 nm. Using a thermo-optical model, we showed that the optical constants of the materials, which are wavelength dependent, as well as their temperature derivatives (dn/dT and dk/dT), strongly influence the thermoreflectance signal. An oscillating pattern is observed in the spectral region where the upper layer is transparent. Such oscillations are due to the interference resulting from the multiple reflections at the interfaces. The optical thicknesses of the layers, mainly determined by the real part of the refractive indices, define the period of oscillation. On the other hand, the imaginary part of the refractive indices establishes the cutoff wavelength of the oscillations. Below this cutoff wavelength, the probe light does not penetrate the material and the upper surface reflectance dominates the signal.

ACKNOWLEDGMENTS

The authors thank A. C. de Oliveira and Professor I. Doi from Centro de Componentes Semicondutores (CCS), Unicamp, for sample preparation. The Brazilian agencies FAPESP, CNPq, and FAEP-Unicamp are also acknowledged for financial support.

[1] J. A. Batista, A. M. Mansanares, E. C. da Silva, and D. Fournier, J. Appl. Phys. **82**, 423 (1997).
[2] L. R. de Freitas, E. C. da Silva, A. M. Mansanares, M. B. C. Pimentel, S. Eleutério Filho, and J. A. Batista, J. Appl. Phys. **97**, 104510 (2005).
[3] P. W. Epperlein, Jpn. J. Appl. Phys., Part 1 **32**, 5514 (1993).
[4] A. M. Mansanares, D. Fournier, and A. C. Boccara, Electron. Lett. **29**, 2045 (1993).
[5] A. M. Mansanares, J. P. Roger, D. Fournier, and A. C. Boccara, Appl. Phys. Lett. **64**, 4 (1994).
[6] L. C. O. Dacal, A. M. Mansanares, and E. C. da Silva, J. Appl. Phys. **84**, 3491 (1998).
[7] A. Mandelis, A. Williams, and E. K. M. Siu, J. Appl. Phys. **63**, 92 (1988).
[8] J. A. Batista, D. Takeuti, A. M. Mansanares, and E. C. da Silva, Anal. Sci. **17**, S73 (2001).
[9] D. Dietzel, H. Roecken, C. Crell, B. K. Bein, and J. Pelzl, Anal. Sci. **17**, S70 (2001).
[10] P. Voigt, J. Hartmann, and M. Reichling, J. Appl. Phys. **80**, 2013 (1996).
[11] S. Grauby, G. Tessier, V. Rachet, S. Hole, and D. Fournier, Anal. Sci. **17**, S67 (2001).
[12] J. A. Batista, A. M. Mansanares, E. C. da Silva, C. C. Vaz, and L. C. M. Miranda, J. Appl. Phys. **88**, 5079 (2000).
[13] A. M. Mansanares, in *Semiconductors and Electronic Materials*, Progress in Photothermal and Photoacoustic Science and Technology Series Vol. IV, edited by A. Mandelis and P. Hess (SPIE Optical Engineering, Bellingham, 2000), Ch. 3, pp. 75–110.
[14] S. Grauby, B. C. Forget, S. Holé, and D. Fournier, Rev. Sci. Instrum. **70**, 3603 (1999).
[15] G. Tessier, S. Holé, and D. Fournier, Appl. Phys. Lett. **78**, 2267 (2001).
[16] G. Tessier, G. Jerosolimski, S. Hole, D. Fournier, and C. Filloy, Rev. Sci. Instrum. **74**, 495 (2003).
[17] B. Batz, in *Modulation Techniques*, Semiconductors and Semimetals Series Vol. 9, edited by R. K. Willardson and Albert C. Beer (Academic, New York, 1972).
[18] G. Busse, D. Wu, and W. Karpen, J. Appl. Phys. **71**, 3962 (1992).
[19] G. E. Jellison, Jr. and F. A. Modine, Phys. Rev. B **27**, 7466 (1983).
[20] G. E. Jellison, Jr. and F. A. Modine, J. Appl. Phys. **76**, 3758 (1994).
[21] A. Borghesi, P. Bottazzi, G. Guizzetti, L. Nosenzo, and A. Stella, Solid State Commun. **60**, 807 (1986).
[22] Ellipsometric measurements made on polycrystalline silicon layer on Si substrate.
[23] Ellipsometric measurements made on SiO_2 layer on Si substrate.
[24] J. R. Reitz, F. J. Milford, and R. W. Christy, *Foundations of Electromagnetic Theory*, 3rd ed. (Addison-Wesley, Massachusetts, 1980).
[25] T. Toyoda and M. Yabe, J. Phys. D **16**, L97 (1983).
[26] R. B. Roberts, J. Phys. D **14**, L163 (1981).
[27] G. K. White, J. Phys. D **6**, 2070 (1973).